Desalination and Water Treatment
www.deswater.com

doi: 10.5004/dwt.2022.28962

277 (2022) 72–84
November

Reuse of sludge from drinking water production in dye wastewater treatment of textile industry

Leila Djekoune[a,*], Zineb Salem[a], Aziz Maaliou[b], Sabrine Boucetta[c], Abdelkader Ouakouak[d]

[a]*Laboratory of Industrial Process Engineering Sciences (LSGPI), Faculty of Mechanical and Process Engineering, University of Sciences and Technology, Houari Boumediene, BP 32 El-Alia, Bâb-Ezzouar, 16311 Algiers, Algeria, emails: ledjekoune@gmail.com (L. Djekoune), zsalem141@gmail.com (Z. Salem)*
[b]*Laboratory of Geotechnical Environment and Hydraulic (LEGHYD), Faculty of Civil Engineering, University of Sciences and Technology, Houari Boumediene, PB 32 El-Alia, Bâb-Ezzouar, 16111 Algiers, Algeria, email: amaaliou@usthb.dz*
[c]*Laboratory of Ecobiology of Marine and Coastal Environments (EMMAL), Badji Mokhtar Annaba University, Algeria, email: sabrine.boucetta@yahoo.com*
[d]*Hydraulic and Civil Engineering Department, University of El Oued, P.O. Box: 789, El Oued 39000, Algeria, email: ouakouakk@yahoo.fr*

Received 10 May 2022; Accepted 25 September 2022

ABSTRACT

The objective of this study was to test the effectiveness of recycled alum sludge, a low-cost material obtained after the coagulation/flocculation process, used as adsorbent to remove an anion dye called Melioderm black AFP 135 (MB-AFP 135) from Rouiba tannery dyeing wastewater (ACED Rouiba). Both of alum sludge and Melioderm black AFP 135 dye were characterized using different analysis methods. The experimental study, carried out in batch, made it possible to study the influence of the operating parameters such as pH solution, alum sludge dosage (C_s), initial dye concentration (C_0) and temperature (T). The results showed that maximal MB-AFP 135 removal of 97% is obtained with: pH = 2, C_s = 2 g/L, C_0 = 100 mg MB-AFP 135 L^{-1} and T = 20°C ± 1°C. The application of different adsorption models showed that the MB-AFP 135 adsorption on alum sludge is well described by Freundlich's and Langmuir's model. The maximum adsorption capacity is estimated at 123.46 mg/g.The data are well correlated with pseudo-second-order kinetic model and MB-AFP 135 adsorption is spontaneous ($\Delta G° < 0$) and endothermic ($\Delta H° > 0$). These experimental results have shown that reusing the alum sludge as a low-cost adsorbent can be considered as a reasonable alternative for such wastewater industry.

Keywords: Alum sludge; Reuse; Tanning industry wastewater; Anionic dye; Adsorption

1. Introduction

Dye-containing industrial wastewater presents a major risk to the environment. With the continuous development of the industrialization process of printing and dyeing, large parts of dyes are released into the environment [1]. It is estimated that only the textile industry can be responsible for the loss of 280.000 tons of dyes in wastewater [2]. Controlling the pollution of this resource has become very important in recent years. For this purpose, several techniques have been used and developed to reduce or eliminate the diffusion of these dyes such as biological degradation, membrane separation, advanced oxidation processes, chemical precipitation, electrochemical and adsorption [3].

* Corresponding author.

Presented at the First International Seminar on Pollution, Health, Environment and Bio-monitoring (SIPSEB-2021), 27–28 December 2021, Virtual Seminar, Skikda, Algeria

Several approaches focused on the adsorption of dyes on different supports. Kaolinite has been effectively used for the removal of Maxilon yellow 4GL and Maxilon red GRL (cationic dyes) [4]. Also, calcite, a natural untreated clay montmorillonite, nickel doped zinc oxide nanoparticles and magnesium phyllosilicate have been effectively used for the removal of anionic dyes [1,5–9].

Alum sludge remains the inevitable by-product of drinking water treatment in water production units when aluminum sulfate is used as a coagulant. The hardness and ferruginous nature of the water to be treated, leads to sludge with more oxides of aluminum, iron, silica and calcium [10]. Beneficial reuse of the material reduces both the cost and the need for disposal.

Alum sludge has recently been used as an effective adsorbent for anions such as phosphate [11,12], arsenate [13], and hexavalent chromium [14] as well as the cations Pb(II) [15] and Hg(II) [16]. Alum sludge was also used as adsorbent for dyes. Nageeb Rashed et al. [17] studied the removal of methylene blue dye from aqueous solution by modified alum sludge. The optimum adsorbent dosage, solution pH, initial dye concentration were 0.25 g/L, 7 and 100 mg/L, respectively.

In this paper, we aim to evaluate the effectiveness of alum sludge in the treatment of anionic dye, Melioderm black AFP 135 (MB-AFP 135) from wastewater tanner industry. The characterization of this material was determined using different analytical methods. Adsorption properties, based on equilibrium adsorption capacity, effect of pH, effect of dye concentration, adsorbent dosage, temperature and contact time on the adsorption process were tested. Kinetic studies were performed and the results were analyzed by applying conventional theoretical methods.

2. Materials and methods

The Melioderm black AFP 135 dye (MB-AFP 135) (type: anionic, solubility: 50 g/L at 20°C, λ_{max} = 605 nm) was supplied from Rouiba Tannery. The chemical composition of MB-AFP 135 was defined using X-ray fluorescence. The functional groups present in this anionic dye were determined by infrared spectroscopy using KBr Alpha Bruker Fourier-transform infrared spectroscopy (FTIR) spectrophotometer in range of 400–4,000 cm^{-1}.

The used alum sludge (AS) was generated after sedimentation process in water treatment plant located in West of Algiers precisely at Reguig–Kaddour. Alum sludge was heated in an oven at 105°C for 24 h. After that, the dried sludge was maintained at room temperature. The sludge particles were then crushed and screened to obtain a particle size smaller than 200 μm.

Elemental chemical analysis of AS was defined using X-ray fluorescence spectroscopy (XRF). FTIR spectra of AS was recorded using KBr Alpha Bruker FTIR spectrometer in range of 400–4,000 cm^{-1}. AS particle morphology was viewed by scanning electron microscopy using an XL30 ESEM at accelerating voltage of 20 kV. The structural characteristics of AS were identified by X-ray diffraction (XRD) using an X'Pert PRO Diffractometer with CuKα radiation (λ = 1.54060 Å) at 45 kV and 40 mA. Scanning diffraction angle is set at the speed of 0.01°/s. The pH at point of zero charge (pH_{ZPC}) was determined by measuring pH at various values, which were obtained using KNO_3 and HCl [18]. The specific surface area (S_{BET}) and volume of pore (V_{Total}) were measured with N_2 absorption–desorption isotherms, using the Brunauer–Emmett–Teller (BET) method [19]. Particle-size distribution was determined with Laser Ray Granulometer in liquid phase (The Malvern Mastersizer 2000 Particle-Size Analyzer).

The stock solution of dye at a concentration of 1 g/L was prepared by dilution in distilled water. Successive dilutions allow obtaining the desired concentrations.

The retention kinetics of MB-AFP 135 on the alum sludge was determined in batch mode. The experiments were performed in an Erlenmeyer flask, containing 50 mL of a dye solution with various initial concentrations (50–500 mg/L). The AS amount varying from 0.5 to 5 g/L was mixed with MB-AFP 135 solution and stirred at 220 rpm. The effect of temperature (10°C–60°C) and solution's pH (1–5), were studied. pH solutions was adjusted by adding NaOH (0.1 mol/L) or HCl (0.1 mol/L). The mixture was continually agitated to reach equilibrium. Then, the suspensions were centrifuged at 4,000 rpm for 4 min and the supernatants were dosed using ultraviolet visible spectrophotometry at λ = 605 nm. Duplicate analyses were performed on each sample.

The dye removal rate (%) was calculated using Eq. (1):

$$R_e(\%) = \frac{(C_0 - C_e) \times 100}{C_0} \quad (1)$$

The adsorption capacity at time t (q_t, mg/g) and equilibrium (q_e, mg/g) was determined from Eqs. (2) and (3):

$$q_t = \left(\frac{C_0 - C_t}{m}\right) \times V_L \quad (2)$$

$$q_e = \left(\frac{C_0 - C_e}{m}\right) \times V_L \quad (3)$$

where C_0, C_t and C_e (mg/L) are respectively: initial concentration, concentration at time t and concentration at equilibrium, m (g) the adsorbent mass, and V (L) is the volume of solution.

3. Results and discussion

3.1. Characterization of MB-AFP 135

The results of the chemical composition of MB-AFP 135 are shown in Table 1.

SO_3, Cl and Na are the dominant components in the dye, with SO_3 being more than 2 times more important than Cl and more than 3 times more important than Na (Table 1). The other elements are present in trace amounts. The dye also contains a significant amount of organic matter, as shown by the LOI value.

The ATR-FTIR spectrum of MB-AFP 135 revealed the presence of azo, sulfonic groups, which are confirmed by the observed bands at 1,588.39; 1,138.13 and 1,041.99 cm^{-1}

respectively (Fig. 1). The attribution of the main observed bands is presented in Table 2.

3.2. Characterization of AS sample

3.2.1. Physico-chemical compositions of AS

The chemical composition analysis of AS: pH, biochemical oxygen demand (BOD_5), moisture content and porosity are summarized in Table 3. The pH value of 8, shows that this sludge is basic. The BOD_5 value reveals that the sludge has a low organic matter; which indicates that it is non-fermentable and stable. The moisture content is very high, while the porosity percentage is about 69%.

From the analytical results in Table 3 it can be seen that the sludge contains the following elements Al, Si, Ca, Fe, S, K, Ti, P, Mg and Na. The predominance of Al, Fe and Ca is due to the use of aluminum sulfate as a coagulant as well as the ferruginous and hard nature of the dam water. The presence of Al, Fe and Ca in sludge is important since the oxides of these elements confer adsorbent properties to this material, which could subsequently explain the phenomena observed during the adsorption process.

3.2.2. X-ray diffraction of AS

The XRD pattern shows that the AS particles are crystalline and not very amorphous and are composed of clay minerals represented by illite and kaolinite and other mineral phases (Fig. 2).

3.2.3. Infrared spectrum of the AS sample

The infrared spectrum of the AS sample is presented in Fig. 3. The broad triplets located at 3,737.11; 3,622 and 3,465.5 cm^{-1} correspond to stretching vibrations of

Table 2
Attribution of the bands in the FTIR spectrum of MB-AFP 135

Wave number (cm^{-1})	Functional group
3,322.48	O–H of phenol
1,588.39	N=N
1,484.13	CH of naphthalene
1,326.01	CH of alkene
1,138.13 and 1,041.99	S=O
838.75	C–H of benzene

Table 3
Properties and chemical composition of AS

Physical property			
pH	8.00		
Moisture (%)	87.35		
SM (%)[a]	12.65		
BOD_5 ($mg{\cdot}O^2/L$)	14.50		
Porosity (%)	68–69		
Chemical composition (%)			
SiO_2	42.09	SO_3	0.34
Al_2O_3	19.73	P_2O_5	0.18
Fe_2O_3	5.57	TiO_2	0.59
CaO	8.21	Mn_2O_3	0.06
Na_2O	0.52	BaO	0.03
MgO	1.34	CuO	0.0084
K_2O	1.74	SrO	0.03
Cl	0.06	LOI	19.78

[a]SM: Solid matter.

Table 1
MB-AFP 135 components

Elements	Value (%)	Elements	Value (%)
SiO_2	0.03	SO_3	29.23
Al_2O_3	<0.01	P_2O_5	0.07
Fe_2O_3	0.07	TiO_2	<0.01
CaO	0.04	Mn_2O_3	<0.01
Na_2O	8.18	NiO	0.0028
MgO	0.05	CuO	0.0084
K_2O	0.02	ZnO	0.0016
Cl	12.34	*LOI	92.21

*LOI: Loss on ignition at 1,000°C.

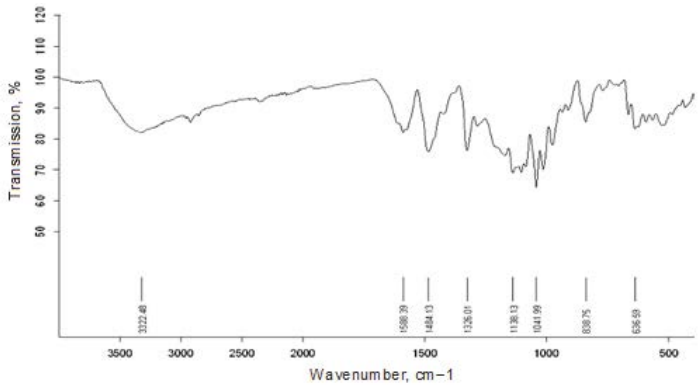

Fig. 1. FTIR spectrum of MB-AFP 135.

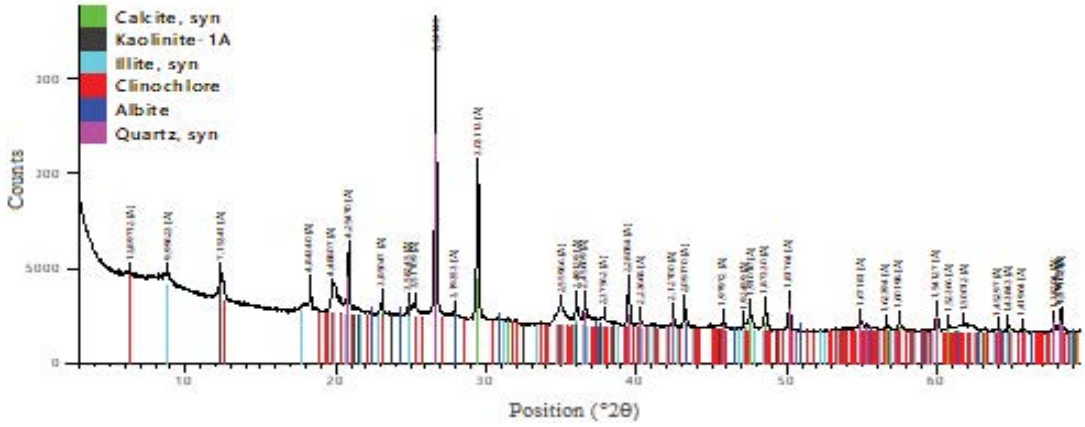

Fig. 2. X-ray diffraction pattern of AS sample.

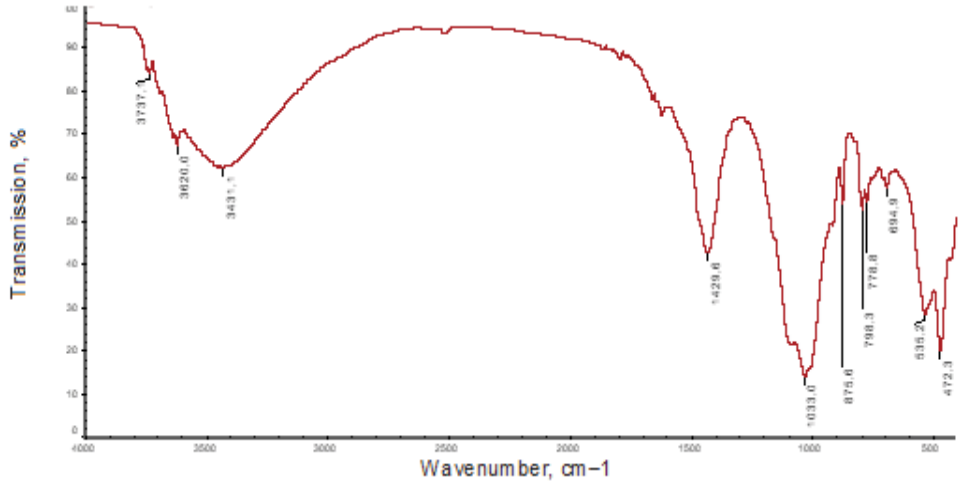

Fig. 3. FTIR spectrum of AS.

the OH functional groups of water. A less intense hook located at 1,429.6 cm^{-1} reveals the presence of CO_3^{2-} from calcite. An intense band at 1,033 cm^{-1} is characteristic of valence vibrations of the Si–O bond of the silicate structure. The rest of the bands between 875.6 and 472.3 cm^{-1} correspond to the stretching vibrations of Si–O, Si–O–Si, OH attached to Al^{3+}, Fe^{3+} and Mg^{2+} groups and to quartz impurities.

3.2.4. Analysis by scanning electron microscopy

Scanning electron microscopy was used to observe the organization and morphology of the sludge particle aggregates. The image obtained by scanning electron microscopy of the alum sludge before adsorption is shown in Fig. 4. This figure shows the presence of the gray particles with irregular forms which are organized in aggregates. The sludge surface also contains a porous network represented by cavities, which are deposited in a random fashion.

3.2.5. Particle-size distribution

The AS contains mainly particles with diameter d = 9.539 μm (90%), 50% of particles have a diameter of 5.894 μm and 10% of particles with diameter d = 3.407 μm (Fig. 5).

3.2.6. Zero-point charge pH (pH_{zpc}) of AS

The point zero charge (pH_{zpc}) of AS (Fig. 6) was found at 7.86. The surface of AS becomes positively charged at pH < pH_{zpc} favoring the adsorption of anionic pollutants, whereas cationic pollutant sorption would be favorable at pH > pH_{zpc} [20]. Point zero charge for AS reported in the literature varies between 5.5 and 6.9 [21].

3.2.7. BET analysis of AS

The sorption–desorption isotherm of the N_2 gas is shown in Fig. 7. According to the IUPAC classification [19], the plot of the N_2 adsorption isotherm belongs to type IV, while the desorption branch shows a large hysteresis loop that occurred over a raised relative pressure range, that is, at P/P_0 = 0.4–0.99.

This result suggests that the AS material had a predominantly mesoporous structure (Vmesopore = 99.32%) with

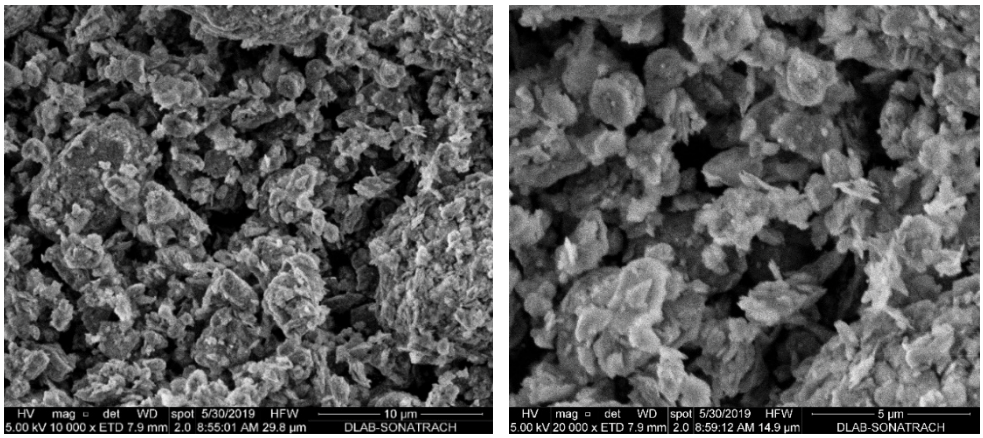

Fig. 4. SEM image of alum sludge.

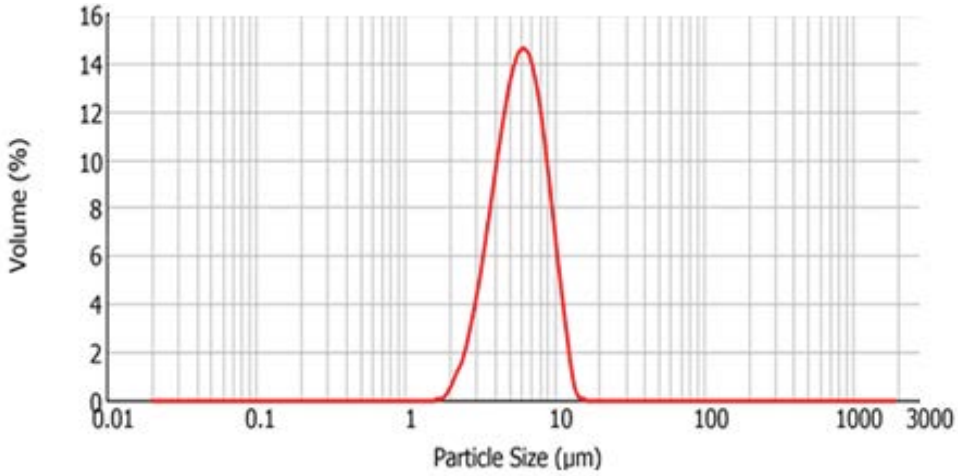

Fig. 5. Distribution of alum sludge particles according to their diameters.

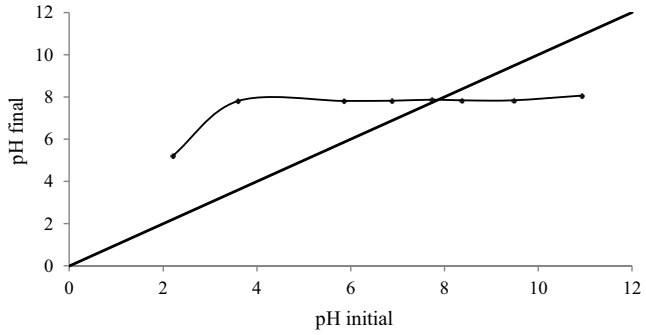

Fig. 6. Zero point charge pH (pH_{zpc}) of AS.

an average pore diameter of 7.86 nm. The data in Fig. 7 also shows that the AS material had a specific surface area (S_{BET} = 29.86 m^2/g and a relatively low total pore volume (V_{Total} = 0.059 cm^3/g).

These results are in agreement with Yang et al. [22], who studied the influence of ageing on the structure and phosphate adsorption capacity of dewatered alum sludge.

3.3. Parametric study of MB-AFP 135 adsorption on AS

3.3.1. Effect of contact time and solution's pH on MB-AFP 135 removal

The contact time effect on MB-AFP 135 removal is shown in Fig. 8. We note that the MB-AFP 135 removal process can be divided into three phases: a first very fast phase is observed in the first 5 min, the dye removal rate exceeds 42%. The kinetics is fast and the dye binds quickly to the easily accessible sites. The second-phase is slow. The number of available sites becomes less and less important. The third phase is the equilibrium phase represented by a plateau, which means the saturation of the pores. The removal rate of MB-AFP 135 reaches 65% after 60 min.

The same result was obtained for methylene blue dye removal onto modified alum sludge [17], and Congo red dye removal by mixed iron oxide-alumina nanocomposites from wastewater [23].

The pH is an important factor in the study of dye adsorption. It can condition both the surface charge of the adsorbent as well as the structure of the dye. The MB-AFP 135 removal on alum sludge as a function of pH

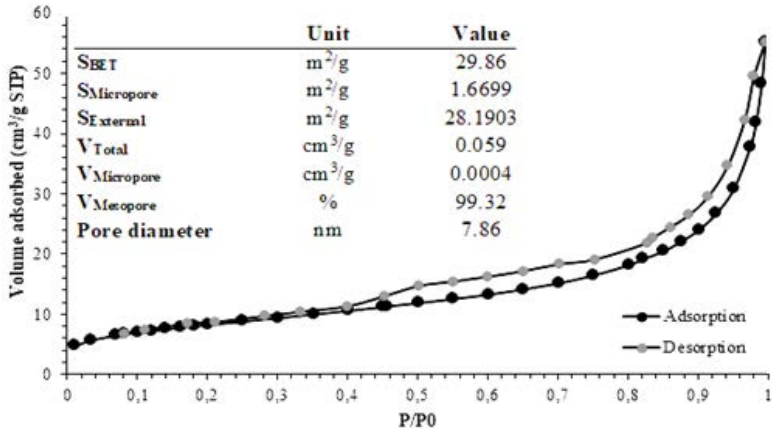

Fig. 7. Nitrogen adsorption–desorption isotherm of AS at 77.4°K and its textural analysis.

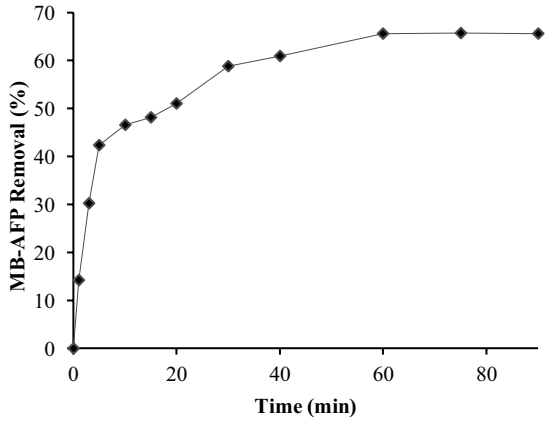

Fig. 8. Effect of contact time on MB-AFP 135 adsorption. (C_0 = 100 mg/L, C_s = 1 g/L, pH = 2.06, T = 20°C ± 1°C, N = 220 rpm).

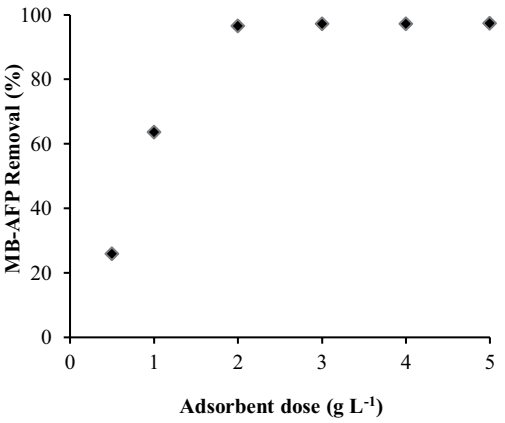

Fig. 10. Effect of adsorbent dose on MB-AFP 135 adsorption. (C_0 = 100 mg/L, pH = 2.11, T = 20°C ± 1°C, N = 220 rpm).

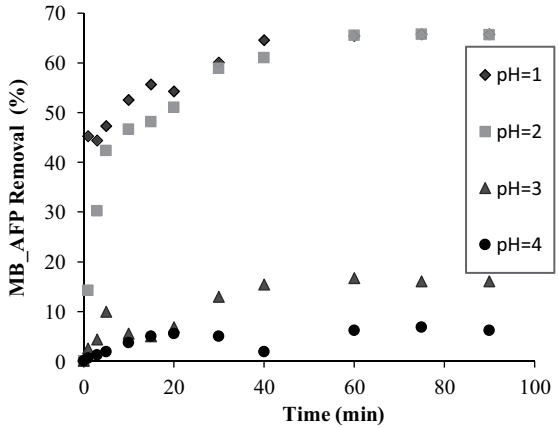

Fig. 9. Effect of pH on MB-AFP 135 adsorption. (C_s = 1 g/L, C_0 = 100 mg/L, T = 21°C ± 1°C, N = 220 rpm).

was studied (Fig. 9). The adsorption rate decreases with increasing pH (from 65.43% for pH 1 to 6.17 for pH 4). We can see from these curves that the maximal adsorption rate of the anionic dye is obtained at pH = 2.

The previous trend can be explained by referring to the results of pH_{zpc} and the equilibrium value of pH solution. At pH ≤ pH_{zpc} (7.86); the positive charge dominates the adsorbent surface. Thus, a significantly high electrostatic attraction exists between the positively charged adsorbent surface and the negative charges of the dye. However, the concentration of positively charges decreases with the increase of the pH values which leads to the decrease of the adsorption efficiency. It can be noted that the equilibrium pH solution increases as the adsorption reaction proceeds, it passes from 2 to 5 when initial pH varies from 1to 4. This could be explained by the fact that when the adsorption process takes place the negative charges occur [24].

Similar result was found by Ozcan et al. [25], Akar and Uysal [26] and Sadri Moghaddam et al. [27].

3.3.2. Effect of adsorbent dose and temperature on MB-AFP 135 removal

Fig. 10 shows the effect of adsorbent dose (0.5, 1, 2, 3, 4 and 5 g/L) on the anion dye adsorption. The MB-AFP 135 removal increases significantly from 25.93% to 96.61% with the adsorbent dose increases from 0.5 to 2.0 g/L and after that, the increase is relatively slow or insignificant.

The enhanced removal with the raised adsorbent dose is due to the increase in the adsorbent surface area and so the presence of more binding sites for adsorption [28]. A slight increase in MB-AFP 135 removal from 96.61% to 97.53% was observed when the AS dose was increased from 2 to 5 g/L.

Abbad and Lounis [29] showed that at high adsorbent dosage, equilibrium was established at an extremely low adsorbate concentration in the solution before reaching saturation. The adsorbent dose was fixed at 2 g/L for the other experiments.

Fig. 11 translates the effect of the temperature on the dye adsorption capacity by AS. It shows that the augmentation of the temperature from 10°C to 60°C increases the retention of the dye from 95% to 97.65%, meaning that the adsorption is endothermic. This evolution was observed also for the Congo red removal (diazo anionic dye) [30] and Methyl orange (anionic dye azo) [31]. The increase in temperature promotes the mobility of anions in solution which improves their exposure to the active sites of the adsorbent. Nthumbi et al. [32] corroborate our obtained results.

3.3.3. Effect of initial dye concentration on MB-AFP 135 removal

In order to study the effect of the initial concentration on the adsorption process, kinetics were performed by contacting 2 g/L of AS with different initial concentrations of the dye (from 25 to 500 mg/L).

The results show that the amount of MB-AFP 135 adsorbed increases with initial dye concentration (Fig. 12). The removal process is fast at the beginning of the contact and becomes slower as equilibrium is approached. The results also reveal that the equilibrium is reached for lower concentrations (<100 mg/L) at 30 min and 60 min for the concentrations above 100 mg/L. Fig. 12 shows that the amount of MB-AFP 135 adsorbed increases from 23.83 to 140 mg/g, for initial concentrations ranging from 50 to 500 mg/g corresponding to a decrease in the adsorption rate from 97.04% to 56.17%. Indeed, for a given adsorbent amount in the solution, the number of active sites is available for setting a limited quantity of adsorbate; this site number is insufficient for higher concentrations [33].

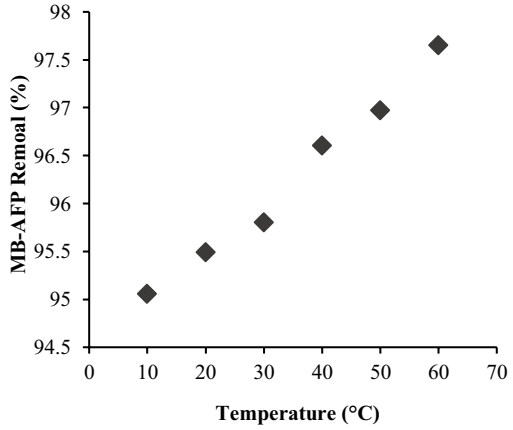

Fig. 11. Effect of temperature on MB-AFP 135 adsorption. (C_s = 2 g/L, C_0 = 100 mg/L, pH = 2.06, N = 220 rpm).

3.4. Modeling of adsorption isotherms (adsorption isotherms)

The adsorption isotherm of MB-AFP 135 on alum sludge is shown in Fig. 13.

According to the classification of Giles et al. [34], the isotherm on AS is L-type. The latter indicates that alum sludge exhibited a high adsorption affinity to MB-AFP 135 in solution. This means that the adsorption efficacy of MB-AFP 135 under low initial concentrations was nearly 99%. Three isotherms model (Langmuir [35], Freundlich and Temkin [36]), as described in equations (4) to (6), were used for fitting the experimental data. (Table 4).

Where q_e is the amount of dye adsorbed per unit of sorbent (mg/g) and C_e is the equilibrium concentration in solution (mg/L). The other parameters are different isotherm constants, which can be determined by regression of the experimental data.

For the purpose of quantitatively comparing the applicability of different adsorption isotherms and kinetics models in fitting to data, the coefficient of correlation and the following error functions were employed [37]:

The coefficient of correlation:

$$R^2 = 1 - \frac{\sum\left(q_{e,\exp} - q_{e,\text{cal}}\right)^2}{\sum\left(q_{e,\exp} - q_{e,\text{mean}}\right)^2} \tag{7}$$

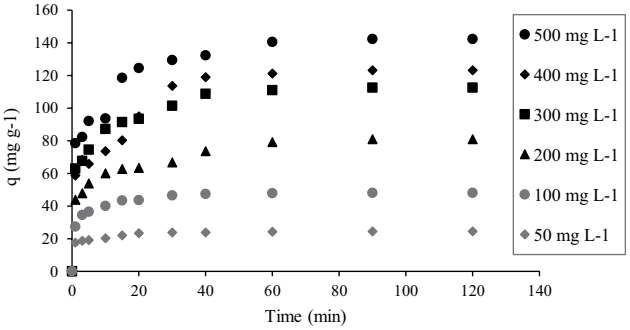

Fig. 12. Effect of initial MB-AFP 135 concentration on adsorption. (C_s = 2 g/L, pH = 1.98, T = 22°C, N = 220 rpm).

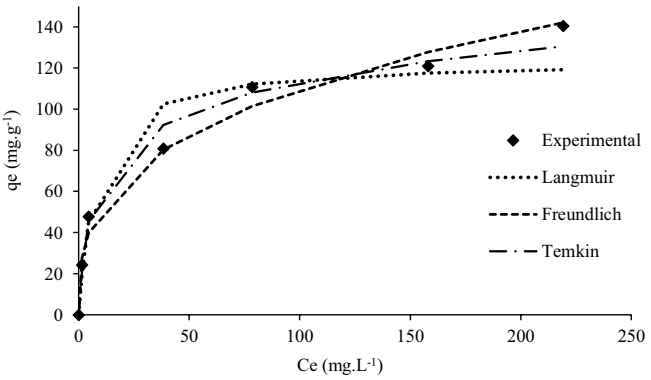

Fig. 13. Experimental results and non-linear relationship of Langmuir, Freundlich and Temkin models. (C_s = 2 g/L, pH = 2.07, T = 20°C ± 1°C, N = 220 rpm).

Table 4
Models of isotherm equation

Isotherm	Non-linear equation	Linear equation	Plot	N° Eq.
Langmuir	$q_e = \frac{q_m K_L C_e}{1 + K_L C_e}$	$\frac{C_e}{q_e} = \frac{1}{q_m} C_e + \frac{1}{K_L q_m}$	$\frac{C_e}{q_e}$ vs. C_e	(4)
Freundlich	$q_e = K_F C_e^{1/n}$	$\ln q_e = \ln K_F + \frac{1}{n} \ln C_e$	$\ln q_e$ vs. $\ln C_e$	(5)
Temkin	$q_e = \frac{RT}{b_T} \ln A_T C_e$	$q_e = \left(\frac{RT}{b_T}\right) \ln A_T + \left(\frac{RT}{b_T}\right) \ln C_e$	q_e vs. $\ln C_e$	(6)

Table 5
Isotherm parameters with error analysis for MB-AFP 135 adsorption on AS

Equation	Parameters	Values
Langmuir I $q_e = \frac{q_m K_L C_e}{1 + K_L C_e}$	q_m (mg/g)	123.46
	K_L (L/mg)	0.128
	R_L	0.057
	R^2	0.987
	χ^2	9.683
	SD	15.497
Freundlich $q_e = K_F C_e^{1/n}$	$1/n_F$	0.331
	k_F (mg/g)(mg/L)$^{1/nF}$	24.38
	R^2	0.990
	χ^2	3.197
	SD	7.199
Temkin $q_e = \frac{RT}{b_T} \ln A_T C_e$	b_T (kJ/mol)	0.112
	R^2	0.864
	χ^2	156.87
	SD	83.667

Standard deviation (SD):

$$\mathrm{SD} = \sqrt{\left(\frac{1}{n-p}\right) \times \left[\sum_{i=1}^{n} \left(q_{e,\exp} - q_{e,\mathrm{cal}}\right)^2\right]} \tag{8}$$

Chi-squared test (χ^2):

$$X^2 = \sum \frac{\left(q_{e,\exp} - q_{e,\mathrm{cal}}\right)^2}{q_{e,\mathrm{cal}}} \tag{9}$$

where $q_{e,\exp}$ and $q_{e,\mathrm{cal}}$ are respectively the experimental values and calculated values by adsorption isotherm, q_{mean} is the mean of q_e experimental values, n and p refer to the number of data points and the number of isotherm parameter, respectively.

The estimated model parameters with the coefficient of correlation R^2 and the error analysis using two different error functions for the different models are given in Table 5. The fitting curves from these three isotherms are also illustrated in Fig. 13.

Similarly, a comparison could be made for two error functions for the different models as illustrated in Fig. 14. It was shown that the experimental data of dye adsorption on alum sludge was well fitted by the Freundlich and Langmuir model. The Freundlich equation suggests the adsorption onto a heterogeneous surface [29]. The Langmuir equation describes monolayer adsorption onto a surface containing a finite number of identical sites. The Freundlich constant value k_F (24.38 (mg/g)(mg/L)$^{1/nF}$) greater than 1, is meaning that the adsorption capacity is high and the value of $1/n_F$ (0.331) between 0 and 1 indicates that the adsorption is favorable in the concentration range [2,38]. For Langmuir, a dimensionless constant equilibrium parameter R_L greater than 0 but less than 1 indicates that Langmuir isotherm is favorable. Based on Langmuir isotherm, the maximum MB-AFP 135 dye adsorption capacity on AS (q_m) is 123.46 mg/g.

A comparison of the maximum dye adsorption capacity on AS with other adsorbents is given in Table 6.

3.5. Adsorption kinetic

The dye adsorption kinetic data were fitted with two kinetic models: pseudo-first-order [41] and pseudo-second-order [42], which were described in Eqs. (10) and (11) respectively:

$$\ln\left(q_e - q_t\right) = \ln\left(q_e\right) - k_1 t \tag{10}$$

$$\frac{t}{q_t} = \frac{1}{k_2 q_e^2} + \frac{t}{q_e} \tag{11}$$

where q_e and q_t are respectively, the dye amounts adsorbed on alum sludge (mg/g) at equilibrium and at time t, k_1 (min^{-1}) and k_2 (g/mg·min) are the rate constant of both pseudo-first-order and pseudo-second-order models. All results obtained are listed in Table 7. Based on correlation coefficient values R^2 and dye amounts at equilibrium, calculated by the two models and compared with the experimental results, it was found that the pseudo-second-order model provided close fit with the MB-AFP 135 removal data.

The calculated kinetics parameters k_2 decrease with increasing initial dye concentration which is in agreement with the experimental curves shown in Fig. 12 due to the change of the equilibrium at high concentrations.

Several studies showed that anion dye adsorption on mineral adsorbents were conducted by pseudo-second-order kinetic model [43]. The second-order model assumes that the adsorption process is of pseudo-second-order and the rate limiting step is chemisorption's. The mechanism may involve sharing of valence forces or through the exchange of electrons between the adsorbent and the adsorbate [44,45].

3.6. Evaluation of thermodynamic parameters of adsorption

Thermodynamic parameters shed valuable insight into feasibility and spontaneity nature of the adsorption process [46].

The thermodynamic parameters are calculated from the following relationship:

$$\Delta G^\circ = -RT\ln K_C \tag{13}$$

$$K_C = \frac{\left(C_0 - C_e\right)}{C_e} \tag{14}$$

$$\ln K_C = \frac{\Delta S^\circ}{R} - \frac{\Delta H^\circ}{RT} \tag{15}$$

where K_C (dimensionless) is the thermodynamic equilibrium constant obtained by multiplying its value by the density of the aqueous solution [47], ΔH°, ΔS° and ΔG° are respectively, the standard enthalpy, the standard entropy and the standard free energy of adsorption. R is the gas constant (8.314 J/K·mol).

By plotting $\ln K_C$ vs. $1/T$ (Fig. 15) the values of ΔH and ΔS were estimated from the slopes and intercepts. Based

Table 7
Kinetic parameters for MB-AFP 135 removal using AS at different initial dye concentration

Parameters of kinetic models	C_0 (mg/L) of dye solution					
	50	100	200	300	400	500
q_{exp} (mg/g)	24.26	47.75	79.01	110.80	120.99	140.43
Pseudo-first-order kinetic model						
q_e (mg/g)	9.37	25.18	40.89	64.97	97.42	76.63
k_1 (min^{-1})	0.088	0.104	0.049	0.077	0.086	0.062
R^2	0.878	0.956	0.842	0.922	0.933	0.895
Pseudo-second-order kinetic model						
q_e (mg/g)	25.00	47.62	79.33	110.92	121.85	140.66
k_2 (g/mg·min)	0.030	0.01	0.0035	0.0033	0.0018	0.0023

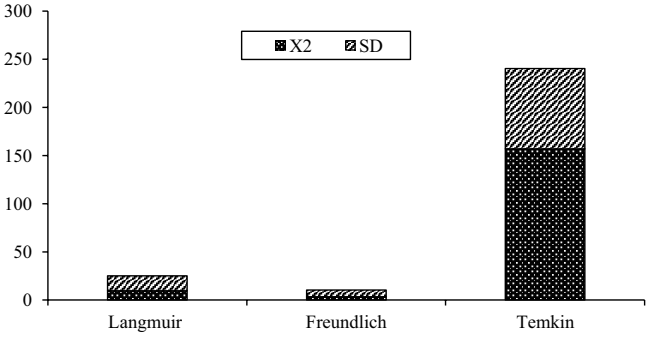

Fig. 14. Comparison of isotherms in the data fitting from error analysis.

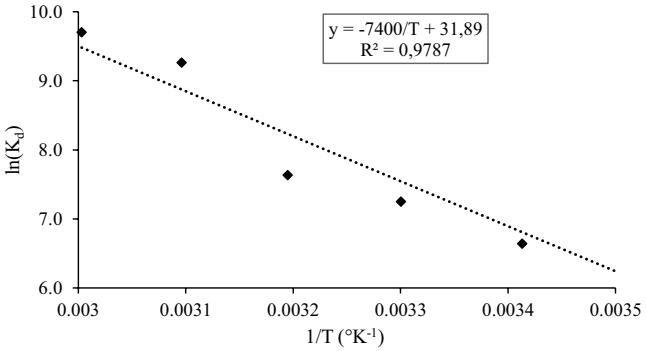

Fig. 15. Evolution of $\ln K_C$ vs. $1/T$.

Table 6
Anions dye capacity adsorption on various adsorbents and their experimental conditions reported in the literature

Adsorbent	Dye	pH	C_0 (mg/L)	T (°C)	q_m (mg/g)	References
Calcite	Acid Black 210	6	10–50	–	210	[1]
Untreated natural clay	Reactive Red 120	5.7	5–25	30	9.7	[5]
Montmorillonite clay	Methyl blue	5	100	35	95.95	[6]
Nickel doped zinc oxide	Methyl orange	4	19–91	35	22.41	[7]
nanoparticles	Tartrazine	6	20–98	20	22.82	
Aminopropyl functionalized magnesium phyllosilicate	Reactive Red 120	2	5–100	25	229.9	[8]
Smectite	Acid Brown 75	2	–	–	8.33	[39]
Chitosan/bentonite hybrid	Amaranth Red	2	100	25	362.1	[40]
composite	Methylene blue	10			496.5	
Alum sludge	Melioderm black AFP 135	2	100	20	123.46	This study

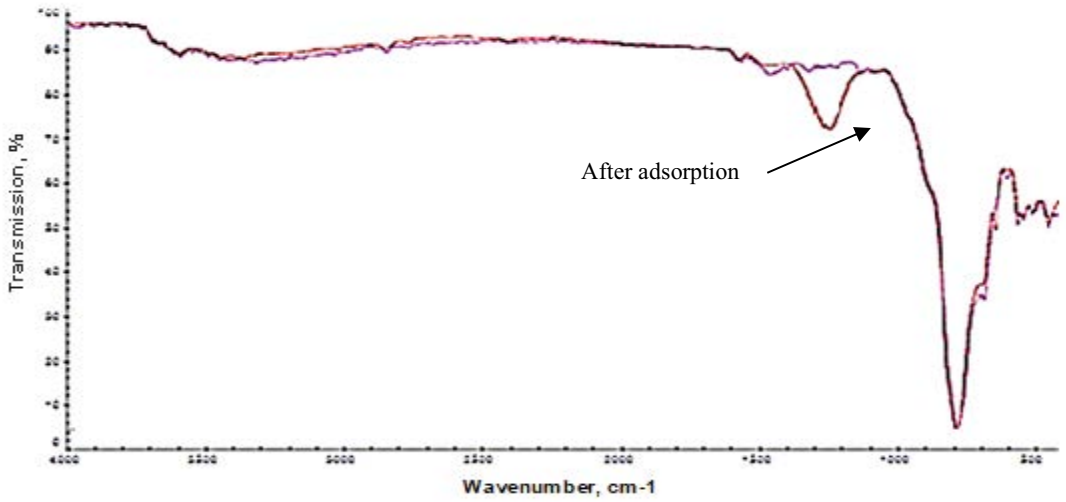

Fig. 16. FTIR spectrum of AS before and after adsorption.

Table 8
Values of the thermodynamic parameters

T (K)	K_C	$\Delta H°$ (kJ/mol)	$\Delta S°$ (kJ/mol·K)	$\Delta G°$ (kJ/mol)
283	641	55.49	0.247	–15.21
293	765			–16.17
303	1,413			–18.27
313	2,065			–19.86
323	10,587			–24.89
333	16,392			–26.87

on the approach, the free energy change (ΔG), enthalpy change (ΔH) and entropy change (ΔS) were calculated for the sorbent (Table 8).

The thermodynamic equilibrium constant K_C increases with the temperature. The free energy ($\Delta G°$) was found negative for the studied temperatures; indicate that this adsorption process is spontaneous in nature and favorably. In addition, the low value of $\Delta G°$ is consistent with electrostatic interaction between adsorption sites and the adsorbing ion (physical adsorption) [48,49]. Malkoc and Nuhoglu [50] noted that the $\Delta G°$ values between 0 and –20 kJ/mol are in the range of multilayer adsorption. According to Erdoğan et al. [51], the positive values of $\Delta H°$ confirm the endothermic nature of adsorption. The positive values of the standard entropy $\Delta S°$ indicate an increase in the freedom degree (or disorder) of the adsorbed species [52].

The FTIR spectra before and after adsorption are almost the same (Fig. 16). However, we notice the appearance of an absorption band of weak intensity located at 1,350 cm^{-1}, which could be attributed to the deformation of the C=O bond.

The XRD analysis of the sludge before and after adsorption (Fig. 17) gave almost the same spectrum except that the calcite concentration decreased. This is probably due to the interaction between the calcite crystals and the dye.

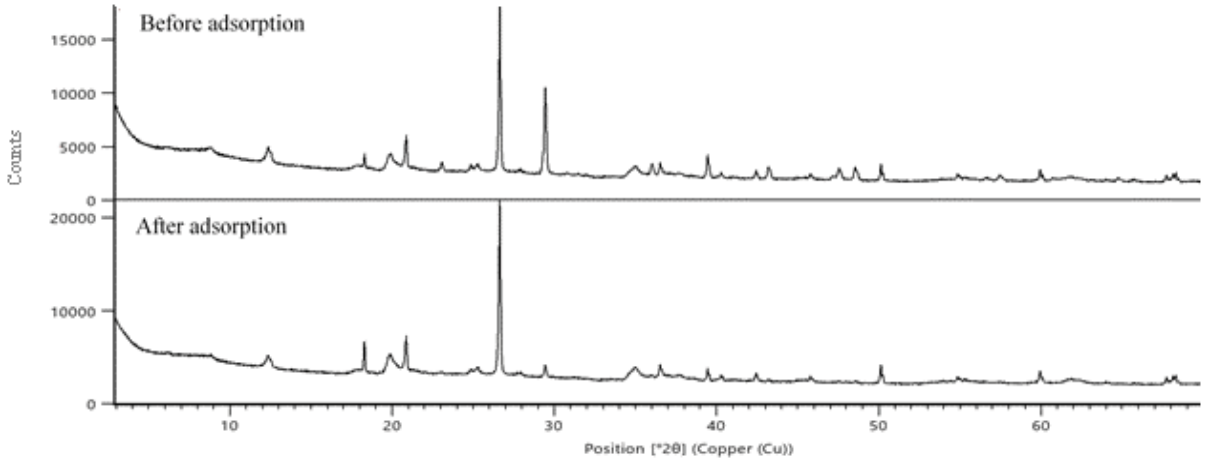

Fig. 17. Diffractogram of the alum sludge before and after adsorption

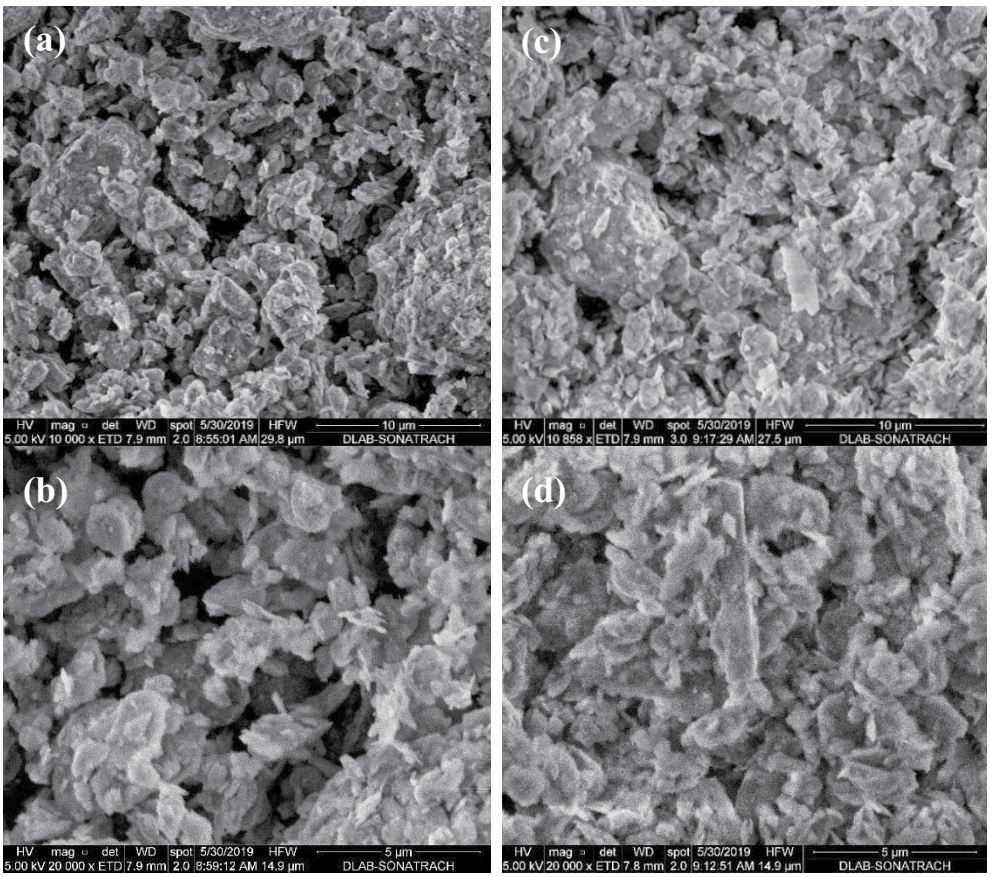

Fig. 18. SEM images of alum sludge: (a,b) before and (c,d) after MB-AFP 135 adsorption.

The scanning electron microscopy (SEM) images obtained for the alum sludge after dye adsorption are presented in Fig. 18. They show an increase in the size of the particle aggregates and became bound together masking the porosity.

4. Conclusion

The aim of this work was to study the removal of an anionic dye (Melioderm black AFP 135) by adsorption using alum sludge. The obtained results show that the alum sludge offers a new and cost effective approach for anion dye removal from aqueous system. The adsorbent samples before and after adsorption have been well characterized by FTIR, XRD and SEM analyses. Adsorption capacity is strongly dependent on initial dye concentration, initial pH and adsorbent dosage.The batch study showed that the maximal dye removal was obtained at acid pH (pH 2). In addition, considering the pH_{zpc} of the adsorbent surface, it was suggested that the main mechanism behind adsorption was through the electrostatic attraction between alum sludge and MB-AFP 135 ions. The kinetic was rapid and the equilibrium was reached after 60 min. The data are well correlated with the kinetic model of the pseudo-second-order. The anionic dye adsorption on alum sludge is well described by Freundlich and Langmuir model, the maximal adsorption capacity was 123.46 mg/g. Thermodynamic results confirm that the adsorption process is spontaneous and endothermic. It can be concluded that the mechanism of adsorption is carried out with physical adsorption. These results show that alum sludge can become an alternative adsorbent due to its low production cost coupled with excellent dye removal.

Symbols

A_T	_	Temkin constant, L/mg
b_T	—	Temkin isotherm constant
E	—	Mean free energy ($E = 1/\sqrt{2K_a}$), kJ/mol
BET	—	Brunauer–Emmett–Teller
B	—	Constant relative to the adsorption heat ($B = RT/b_T$), J/mol
C_0	—	Initial solute concentration, mg/L
C_e	—	Solute concentration at equilibrium, mg/L
C_s	—	Concentration of alum sludge in solution, g/L
C_t	—	Solute concentration at time t, mg/L
K_L	—	Langmuir constant, L/mg
k_F	—	Freundlich isotherm constant, k_F (mg/g)(mg/L)$^{1/nF}$
k_1	—	Rate constant for a pseudo-first-order kinetics, s^{-1}
k_2	—	Rate constant for the pseudo-second-order kinetics, s^{-1}
m	—	Mass of alum sludge, mg
$1/n_F$	—	Heterogeneity factor

q_e — Adsorption capacity at equilibrium, mg/g
q_m — Maximum capacity of adsorption, mg/g
q_t — Adsorption capacity at time t, mg/g
R — Universal gas constant (8.314 J/mol·K), J/mol·K
R^2 — Correlation coefficient
T — Temperature, Kelvin
V — Solution volume, mL
N — Stirring velocity, rpm
$\Delta H°$ — Standard enthalpy, kJ/mol
$\Delta S°$ — Standard entropy, kJ/mol·K
$\Delta G°$ — Standard free enthalpy, kJ/mol
K_C — Thermodynamic equilibrium constant

References

[1] A. Talhi, S. Merabet, L. Bouhouf, C. Boukhalfa, Removal of Acid Black 210 by adsorption on calcite, Desal. Water Treat., 205 (2020) 407–411.
[2] M.P. da Rosa, A.V. Igansi, S.F. Lütke, T.R. Sant'Anna Cadaval Jr., A.C.R. do Santos, A.P. de Oliveira Lopes Inacio, L.A. de Almeida Pinto, P.H. Beck, A new approach to convert rice husk waste in a quick and efficient adsorbent to remove cationic dye from water, J. Environ. Chem. Eng., 7 (2019) 103504, doi: 10.1016/j.jece.2019.103504.
[3] I. Lansari, B. Benguella, N. Kruchinina, A. Nistratov, Adsorption of a textile dye from aqueous solution on natural and modified sawdust, Desal. Water Treat., 194 (2020) 259–268.
[4] M. Doğan, M. Hamdi Karaoğlu, M. Alkan, Adsorption kinetics of maxilon yellow 4GL and maxilon red GRL dyes on kaolinite, J. Hazard. Mater., 165 (2009) 1142–1151.
[5] E. Errais, J. Duplay, F. Darragi, I. M'Rabet, A. Aubert, F. Huber, G. Morvan, Efficient anionic dye adsorption on natural untreated clay: kinetic study and thermodynamic parameters, Desalination, 275 (2011) 74–81.
[6] P. Sharma, D.J. Borah, P. Das, M.R. Das, Cationic and anionic dye removal from aqueous solution using montmorillonite clay: evaluation of adsorption parameters and mechanism, Desal. Water Treat., 57 (2015) 8372–8388.
[7] C. Klett, A. Barry, I. Balti, P. Lelli, F. Schoenstein, N. Jouini, Nickel doped zinc oxide as a potential sorbent for decolorization of specific dyes, methylorange and tartrazine by adsorption process, J. Environ. Chem. Eng., 2 (2014) 914–926.
[8] Y.-W. Kim, J.-H. Kim, D.H. Moon, H.-J. Shin, Adsorption and precipitation of anionic dye Reactive Red 120 from aqueous solution by aminopropyl functionalized magnesium phyllosilicate, Korean J. Chem. Eng., 36 (2019) 101–108.
[9] W. Rao, P. Piliouras, X. Wang, A. Guido, K. Kugler, B. Sieren, L. Wang, G. Lv, Z. Li, Zwitterionic dye rhodamine B (RhB) uptake on different types of clay minerals, Appl. Clay Sci., 197 (2020) 105790, doi: 10.1016/j.clay.2020.105790.
[10] Y. Yang, Y.Q. Zhao, A.O. Babatunde, L. Wang, Y.X. Ren, Y. Han, Characteristics and mechanisms of phosphate adsorption on dewatered alum sludge, Sep. Purif. Technol., 51 (2006) 193–200.
[11] Y. Zhao, Q. Yue, Q. Li, X. Xu, Z. Yang, X. Wang, B. Gao, H. Yu, Characterization of red mud granular adsorbent (RMGA) and its performance on phosphate removal from aqueous solution, Chem. Eng. J., 193–194 (2012) 161–168.
[12] A.O. Babatunde, Y.Q. Zhao, X.H. Zhao, Alum sludge-based constructed wetland system for enhanced removal of P and OM from wastewater: concept, design and performance analysis, Bioresour. Technol., 101 (2010) 6576–6579.
[13] K.C. Makris, D. Sarkar, R. Datta, Evaluating a drinking-water waste by-product as a novel sorbent for arsenic, Chemosphere, 64 (2006) 730–741.
[14] Y.-F. Zhou, R.J. Haynes, Removal of Pb(II), Cr(III) and Cr(VI) from aqueous solutions using alum-derived water treatment sludge, Water Air Soil Pollut., 215 (2011) 631–640.
[15] W. Chu, Lead metal removal by recycled alum sludge, Water Res., 33 (1999) 3019–3025.
[16] A. Hovsepyan, J.-C.J. Bonzongo, Aluminum drinking water treatment residuals (Al-WTRs) as sorbent for mercury: implications for soil remediation, J. Hazard. Mater., 164 (2009) 73–80.
[17] M. Nageeb Rashed, M.A. El-Daim El Taher, S.M.M. Fadlalla, Adsorption of methylene blue using modified adsorbents from drinking water treatment sludge, Water Sci. Technol., 74 (2016) 1885–1898.
[18] S.K. Mishra, S.B. Kanungo, Rajeev, Adsorption of sodium dodecyl benzenesulfonate onto coal, J. Colloid Interface Sci., 247 (2003) 42–48.
[19] K.S.W. Sing, R.T. Williams, Physisorption hysteresis loops and the characterization of nanoporous materials, Adsorpt. Sci. Technol., 22 (2004) 773–782.
[20] A.-A. Peláez-Cid, A.-M. Herrera-González, M. Salazar-Villanueva, A. Bautista-Hernández, Elimination of textile dyes using activated carbons prepared from vegetable residues and their characterization, J. Environ. Manage., 181 (2016) 269–278.
[21] Y.-F. Zhou, R.J. Haynes, Removal of Pb(II), Cr(III) and Cr(VI) from aqueous solutions using alum-derived water treatment sludge, Water Air Soil Pollut., 215 (2011) 631–640.
[22] Y. Yang, Y.Q. Zhao, P. Kearney, Influence of ageing on the structure and phosphate adsorption capacity of dewatered alum sludge, Chem. Eng. J., 145 (2008) 276–284.
[23] A. Mahapatra, B.G. Mishra, G. Hota, Adsorptive removal of Congo red dye from wastewater by mixed iron oxide–alumina nanocomposites, Ceram. Int., 39 (2013) 5443–5451.
[24] M. Hasnain Isa, L. Siew Lang, F.A.H. Asaari, H.A. Aziz, N. Azam Ramli, J.P.A. Dhas, Low cost removal of disperse dyes from aqueous solution using palm ash, Dyes Pigm., 74 (2007) 446–453.
[25] A. Ozcan, C. Omeroğlu, Y. Erdoğan, A.S. Ozcan, Modification of bentonite with a cationic surfactant: an adsorption study of textile dye Reactive Blue 19, J. Hazard. Mater., 140 (2007) 173–179.
[26] S.T. Akar, R. Uysal, Untreated clay with high adsorption capacity for effective removal of C.I. Acid Red 88 from aqueous solutions: batch and dynamic flow mode studies, Chem. Eng. J., 162 (2010) 591–598.
[27] S. Sadri Moghaddam, M.R. Alavi Moghaddam, M. Arami, Coagulation/flocculation process for dye removal using sludge from water treatment plant: optimization through response surface methodology, J. Hazard. Mater., 175 (2010) 651–657.
[28] A. Gürses, Ç. Doğar, M. Yalçın, M. Açıkyıldız, R. Bayrak, S. Karaca, The adsorption kinetics of the cationic dye, methylene blue, onto clay, J. Hazard. Mater., 131 (2006) 217–228.
[29] B. Abbad, A. Lounis, Removal of methylene blue from colored effluents by adsorption onto ZnAPSO-34 nanoporous material, Desal. Water Treat., 52 (2014) 7766–7775.
[30] S. Sinha, S.S. Behera, S. Das, A. Basu, R.K. Mohapatra, B.M. Murmu, N.K. Dhal, S.K. Tripathy, P.K. Parhi, Removal of Congo Red dye from aqueous solution using Amberlite IRA-400 in batch and fixed bed reactors, Chem. Eng. Commun., 205 (2018) 432–444.
[31] S.S. Behera, S. Das, P.K. Parhi, S.K. Tripathy, R.K. Mohapatra, M. Debata, Kinetics, thermodynamics and isotherm studies on adsorption of methyl orange from aqueous solution using ion exchange resin Amberlite IRA-400, Desal. Water Treat., 60 (2017) 249–260.
[32] R.M. Nthumbi, J.C. Ngila, B. Moodley, A. Kindness, L. Petrik, Application of chitosan/polyacrylamide nanofibres for removal of chromate and phosphate in water, Phys. Chem. Earth Part A/B/C, 50–52 (2012) 243–251.
[33] K. Vasanth Kumar, V. Ramamurthi, S. Sivanesan, Modeling the mechanism involved during the sorption of methylene blue onto fly ash, J. Colloid Interface Sci., 284 (2005) 14–21.
[34] C.H. Giles, D. Smith, A. Huitson, A general treatment and classification of the solute adsorption isotherm. I. Theoretical, J. Colloid Interface Sci., 47 (1974) 755–765.
[35] I. Langmuir. The constitution and fundamental properties of solids and liquids. Part I. Solids, J. Am. Chem. Soc., 38 (1916) 2221–2295.

[36] K.Y. Foo, B.H. Hameed, Insights into the modeling of adsorption isotherm systems, Chem. Eng. J., 156 (2010) 2–10.
[37] A. Ouakouak, M. Abdelhamid, B. Thouraya, H.-O. Chahinez, G. Hocine, N. Hamdi, A. Syafiuddin, R. Boopathy, Development of a novel adsorbent prepared from dredging sediment for effective removal of dye in aqueous solutions, Appl. Sci., 11 (2021) 10722, doi: 10.3390/app112210722.
[38] K. Khelif, Z. Salem, L. Boumehdi, Nutrient removal from wastewaters using treated incineration residues of expired medications: kinetics, thermodynamics and isotherm modeling, Part. Sci. Technol.: An Int. J., 36 (2018) 560–568.
[39] I. Chaari, E. Fakhfakh, M. Medhioub, F. Jamoussi, Comparative study on adsorption of cationic and anionic dyes by smectite rich natural clays, J. Mol. Struct., 1179 (2019) 672–677.
[40] G.L. Dotto, F.K. Rodrigues, E.H. Tanabe, R. Fröhlich, D.A. Bertuol, T.R. Martins, E.L. Foletto, Development of chitosan/bentonite hybrid composite to remove hazardous anionic and cationic dyes from colored effluents, J. Environ. Chem. Eng., 4 (2016) 3230–3239.
[41] S. Lagergren, About the theory of so-called adsorption of soluble substances, Kungliga Svenska Vetenskapsakademiens, Handlingar, Band, 24 (1898) 1–39.
[42] Y.S. Ho, G. McKay, Pseudo-second-order model for sorption processes, Process Biochem., 34 (2000) 451–465.
[43] M.T. Yagub, T.K. Sen, S. Afroze, H.M. Ang, Dye and its removal from aqueous solution by adsorption: a review, Adv. Colloid Interface Sci., 209 (2014) 172–184.
[44] M. Khitous, Z. Salem, D. Halliche, Removal of phosphate from industrial wastewater using uncalcined MgAl-NO_3 layered double hydroxide: batch study and modeling, Desal. Water Treat., 57 (2016) 15920–15931.
[45] Z. Bekçi, Y. Seki, M. Kadir Yurdakoç, Equilibrium studies for trimethoprim adsorption on montmorillonite KSF, J. Hazard. Mater., 133 (2006) 233–242.
[46] E. Nassef, Removal of phosphates from industrial wastewater by chemical precipitation, IRACST – Eng. Sci. Technol.: An Int. J. (ESTIJ), 2 (2012) 409–413.
[47] E.C. Lima, A. Hosseini-Bandegharaei, J.C. Moreno-Piraján, I. Anastopoulos, A critical review of the estimation of the thermodynamic parameters on adsorption equilibria. Wrong use of equilibrium constant in the Van't Hoof equation for calculation of thermodynamic parameters of adsorption, J. Mol. Liq., 273 (2019) 425–434.
[48] J.M. Smith, H.C. Van Ness, Introduction to Chemical Engineering Thermodynamics, 4th ed., McGraw-Hill, Singapore, 1987.
[49] D. Singh, Studies of the adsorption thermodynamics of oxamyl on fly ash, Adsorpt. Sci. Technol., 18 (2000) 741–748.
[50] E. Malkoc, Y. Nuhoglu, Determination of kinetic and equilibrium parameters of the batch adsorption of Cr(VI) onto waste acorn of *Quercus ithaburensis*, Chem. Eng. Process. Process Intensif., 46 (2007) 1020–1025.
[51] S. Erdoğan, C.A. Başar, Y. Önal, Particle size effect of raw material on the pore structure of carbon support and its adsorption capability, Part. Sci. Technol.: An Int. J., 35 (2016) 330–337.
[52] J. Das, B.S. Patra, N. Baliarsingh, K.M. Parida, Adsorption of phosphate by layered double hydroxides in aqueous solutions, Appl. Clay Sci., 32 (2006) 252–260.